ROYAL SOCIETY OPEN SCIENCE

royalsocietypublishing.org/journal/rsos

Research

Cite this article: Lu WZ, Lu HF, Zhang ZK. 2019 TiO_2-SiO_2 supported $MnWO_x$ catalysts by liquid-phase deposition for low-temperature NH_3-SCR. *R. Soc. open sci.* **6**: 180669.
http://dx.doi.org/10.1098/rsos.180669

Received: 4 May 2018
Accepted: 18 December 2018

Subject Category:
Chemistry

Subject Areas:
physical chemistry

Keywords:
NH_3-SCR, $MnWO_4$, TiO_2-SiO_2, liquid-phase deposition, low temperature

Author for correspondence:
Zekai Zhang
e-mail: zzk@zjut.edu.cn

This article has been edited by the Royal Society of Chemistry, including the commissioning, peer review process and editorial aspects up to the point of acceptance.

THE ROYAL SOCIETY PUBLISHING

TiO_2-SiO_2 supported $MnWO_x$ catalysts by liquid-phase deposition for low-temperature NH_3-SCR

Weizhe Lu, Hanfeng Lu and Zekai Zhang

Institute of Catalytic Reaction Engineering, College of Chemical Engineering, Zhejiang University of Technology, Hangzhou 310014, People's Republic of China

ZZ, 0000-0002-4136-5263

NH_3-SCR is an environmentally important reaction for the abatement of NO_x from different resources. MnO_2-based catalyst has attracted significant attention due to the excellent activity. In this paper, a series of $MnWO_x/TiO_2-SiO_2$ catalysts were prepared by liquid-phase deposition method. The catalysts were characterized by N_2 adsorption/desorption, XRD, TEM, XPS, FT-IR, H_2-TPR, TG and water adsorption capacity. The existence of SiO_2 improved the SO_2 and H_2O resistance of the $MnWO_x/TiO_2-SiO_2$ catalyst without decreasing the NH_3-SCR activity. Under the reaction conditions of 260°C and 60 000 ml g_{cata} h^{-1} gas hourly space velocity (GHSV), the NO conversion was kept stable at about 95% for 140 min on stream. The excellent performance of $MnWO_x/TiO_2-SiO_2$ catalyst is considered to be originated from the texture properties and active species dispersion improvement by SiO_2 in the support and low-temperature preparation.

1. Introduction

Nitrogen oxides are one of the major pollutants that endanger the atmosphere air, which can cause severe environmental problems such as acid rain, smog and photochemical pollution. deNO_x is a hot topic in the environmental fields in the past decades, and many researchers continue to be concerned till present. Comparing to the other routes, it is a desirable way to reduce NO_x to harmless N_2. Selective catalytic reduction of NO_x via NH_3 (NH_3-SCR) thereby has been widely studied and applied in the elimination of nitrogen oxides [1,2].

In general, NO_x are mainly released from the combustion of fossil fuels at different stationary or mobile resources. The nature of the two types of exhaust gases is quite different. The catalysts are also evolved into two series, the transition metal oxide-based catalysts for the stationary resources, and the

zeolite-based catalysts for the mobile resources. V_2O_5-$WO_3(MoO_3)/TiO_2$ as the representative of the vanadium-based metal oxide catalyst has been commercialized and widely used in industry [3,4]. The working temperature window of V_2O_5-$WO_3(MoO_3)/TiO_2$ is mainly in the temperature range of 300–400°C, and it cannot completely remove NO_x below 250°C. The working temperature window means a strict requirement for working conditions and high energy consumption [5]. Therefore, it attracts many researchers to find new catalyst systems that can operate at lower temperatures.

Among newly developed catalyst systems, Mn and Ce oxide-based catalysts have shown outstanding performance [6–11]. Especially, manganese-oxide-based catalysts can achieve very high NO_x conversion even below 100°C temperature, which makes them a very competitive alternative NH_3-SCR catalysts system [12,13]. However, the main shortcoming of Mn-based catalysts is the poor resistance to the SO_2 in the exhaust gases. Therefore, Ce-based catalysts, especially Ce-W mixed oxides catalysts, attracted some more attention in the very recent years. At present, the commonly accepted catalyst for SO_2 poisoning is that a large amount of sulfate is formed, which blocks the catalyst pores and inactivates the active sites. Li's and He's groups have done a lot of research and made notable progress [14–17].

Meanwhile, Mn-based catalysts are still worthy to be studied as long as the sulfur resistance is improved. By investigation, it is found that tungsten may possess the ability. Tungsten has been added and helped for the V, Ce-based catalysts, and even for the NiWS catalyst in the hydrodesulfurization process [18,19]. Liu *et al.* first considered $MnWO_x$ as the main active phase and got high deNO_x efficiency from 60 to 250°C [20]. Sun *et al.* then prepared a series of $W_\alpha Mn_{1-\alpha}O_x$ catalysts via coprecipitation method [21]. $W_{0.33}Mn_{0.66}O_x$ catalyst with amorphous or poorly crystalline Mn and W species showed the highest NH_3-SCR activity within a broad temperature range of 230–470°C. Our group also prepared the $MnWTiO_{2-\delta}$ catalyst with $MnWO_4$ crystal structure and obtained a high activity in the range of 200–400°C [22,23].

The deactivation of the NH_3-SCR catalyst mainly comes from two aspects, the poisoning caused by the reaction of SO_2 with the active components, and the coverage or blocking (coking) of the surface of the ammonium sulfate [24–26]. Owing to the viscosity of NH_4HSO_4 and $(NH_4)_2SO_4$, it is easy to bind to the catalyst and reduce the specific surface area. The formation of NH_4HSO_4 and $(NH_4)_2SO_4$ often needs water. If the surface has well-hydrophobic properties, it would be possible to reduce the water adsorption and thus decrease the formation of NH_4HSO_4 and $(NH_4)_2SO_4$; i.e. the sulfur resistance of the catalyst is expected to be improved by increasing the hydrophobicity of the catalyst surface [27,28].

In this work, a series of TiO_2–SiO_2-supported $MnMO_x$ catalysts were prepared by a liquid-phase deposition (LPD) method. The introduction of SiO_2 increases the specific surface area of the catalyst; moreover, probably by the reaction of manganese nitrate and ammonia tungstate to form $MnWO_4$, the catalysts could be prepared at relatively low temperature, which greatly improves the activity and N_2 selectivity of the $MnWO_x/TiO_2$–SiO_2 catalyst as well as the SO_2 and H_2O resistance.

2. Experimental procedure

2.1. Catalyst preparation

$MnWO_x/TiO_2$–SiO_2 catalysts were prepared by two main procedures. The first step is to prepare TiO_2–SiO_2 support by a sol–gel method. The method used TEOS (*n*-ethyl silicate) and TBOT (tetrabutyl titanate) as precursors. Taking 10% SiO_2–90% TiO_2 as an example, a suitable amount of TEOS (1.0 ml) was mixed in anhydrous ethanol, then a small amount of distilled water (about 2.0 ml) and several drops of 1 mol l^{-1} HCl were added stirring for 30 min at room temperature to adjust pH = 2 and got solution A. Meanwhile, 5.0 ml of acetic acid was mixed with 49.0 ml anhydrous ethanol, then a small amount of distilled water (about 2.0 ml) and several drops of 1 mol l^{-1} HCl were added to adjust pH ≤ 3 and got solution B. Solutions A and B were then uniformly mixed by stirring to get solution C. Then 13.5 ml anhydrous ethanol and 13.5 ml TBOT were uniformly mixed to get solution D. Solution D was added into solution C at a rate of 3 ml min^{-1} under vigorous stirring at room temperature. The resulting material was dried in an oven at 80°C for 12 h to obtain the TiO_2–SiO_2 dry gel. The gel was ground into powder to obtain the support.

Considering the dispersion of active components on the hydrophobic support, a modified liquid deposition method was used to load the $MnWO_x$ on the TiO_2–SiO_2. Manganese nitrate solution (50% $Mn(NO_3)_2$) and tungaline ($(NH_4)_{10}W_{12}O_{41}\cdot xH_2O$) were used as precursors; 0.845 g $(NH_4)_{10}W_{12}O41\cdot xH_2O$ and 2.386 g $Mn(NO_3)_2$ solution were dissolved with the same molar oxalic acid in deionized water. TiO_2–SiO_2 powder was added to the solution and the mixture was vigorous stirred

for 1 h. Ammonia water (0.5 mol l^{-1}) was slowly added into the mixture to adjust the pH to 10 to achieve the precipitation of active species. The mixture was filtered, washed and the precipitate in the oven was dried at 110°C for 12 h. At last, the sample was moved into the muffle and calcined at 200°C for 2 h to obtain the target $MnWO_x/TiO_2–SiO_2$ catalyst. The samples were labelled as $Mn_xW_yO_x/TiO_2–SiO_2(n)$, where x and y are the molar ratio of Mn : W and n is the percentage of SiO_2 to ($SiO_2 + TiO_2$).

2.2. Catalyst characterization

N_2 adsorption/desorption of the catalysts were measured by a Micromeritics 3Flex physical adsorption instrument. The samples were heated to 200°C under vacuum pressure and kept for 10 h before measurement. Specific surface area was calculated using the BET method.

Crystal structure of the catalysts were detected by an ARL SCINTAG X'TRA instrument (Shimadzu.) using Cu Kα radiation in 2θ range of 10–80° with a step size of 0.02°.

H_2 temperature-programmed reduction (H_2-TPR) was conducted on a chemical adsorption apparatus (Finetec Corp.). The samples were pretreated at 400°C in Ar for 40 min. The TPR analysis was carried out in a reducing gas mixture (30 ml min^{-1}) consisting of 5% H_2 and balance Ar from 60 to 800°C at a rate of 10°C min^{-1}. TCD detector temperature was 60°C.

X-ray photoelectron spectroscopy (XPS) was conducted on a Kratos AXIS Ultra DLD clutches spectrophotometer. Excitation source was the monochromatic Al Kα radiation ($h\upsilon = 1486.6$ eV). The power was 45 W. The working voltage was 15 kV. Scanning area was 300 × 700 μm. Vacuum test was better than the 8.5×10^{-9} mbar. The data were corrected using the C1 s 284.8 eV as the standard.

Skeleton FT-IR spectra of the catalysts were recorded using BRUKER VERTEX70 FT-IR apparatus, with the sample in KBr pellets.

Morphologies of the catalysts were disclosed by a Philips-FEI company Tecnai G2F30 S-Twin type high-resolution transmission electron microscopy. The samples were solved in ethanol solution to get the dispersed particles. The accelerating voltage was 300 kV.

The water adsorption capacity of the catalysts was determined by the saturated water adsorption experiment. The appropriate amount of dry sample was put into a weighing bottle and placed in a saturated water vapour environment. After the adsorption is balanced, the mass change was weighed with a electronic balance.

The coke of the catalyst after the reaction was analysed by an STA449 integrated thermal analyser. A total of 0.100 g of the sample was placed in an alumina crucible and heated from room temperature to 1000°C at a rate of 20°C min^{-1} in a 20% O_2/80% N_2 atmosphere.

2.3. Catalytic activity tests

NH_3-SCR activity was tested in a fixed-bed quartz tube reactor (i.d. = 8 mm). The reaction conditions were as follows: 500 ppm of NO, 500 ppm of NH_3, 5.0% O_2 and N_2 as balance, 10 vol% H_2O (when used), 100 ppm SO_2 (when used). Total gas flow rate was about 500 ml min^{-1}, and calculated gas hourly space velocity (GHSV) of 60 000 ml g_{cata} h^{-1}. Outlet gases were measured by an online MODEL T200H/M nitrogen analyser and Thermo trace 1300 gas chromatography. NO conversion (X) and N_2 selectivity (S) were calculated by the following equations:

$$X(\%) = \frac{([NO]_{in} - [NO]_{out})}{[NO]_{in}} \tag{2.1}$$

and

$$S(\%) = \frac{(([NO]_{in}+[NH_3]_{in}) - [NO_2]_{out} - 2[N_2O]_{out})}{([NO]_{in}+[NH_3]_{in})}. \tag{2.2}$$

3. Results and discussions

3.1. NH_3-SCR activity of $MnWO_x/TiO_2-SiO_2$ and effect of preparation conditions

Prior to this paper, the $MnWO_x/TiO_2$ catalysts are mainly prepared by self-propagating high-temperature synthesis method (SHS) in our group, because the as-prepared samples possess very good properties such as narrow particle distribution and uniformly distributed $MnWO_x$ species on the TiO_2 support. However, it seems that the method is not very suitable for $TiO_2–SiO_2$ support. The

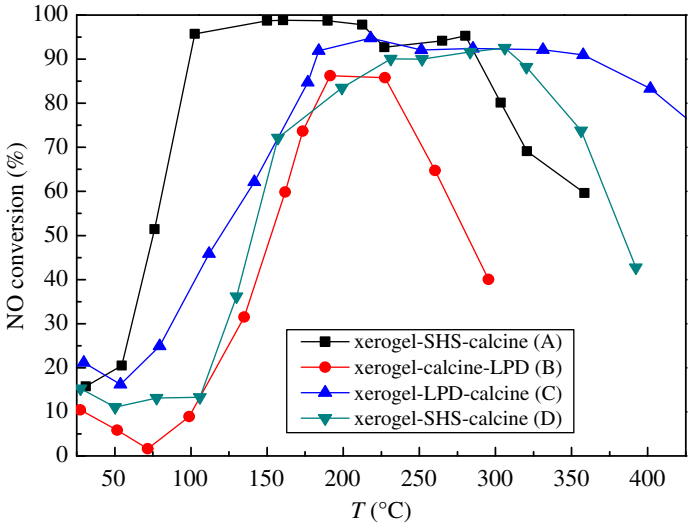

Figure 1. NH_3-SCR activity of Mn_2WO_x/TiO_2-SiO_2 with different preparation steps.

sample temperature could rise to very high (greater than 1000°C) during the preparation process and affect the pore structure of the TiO_2-SiO_2 support.

Figure 1 shows that the activity of $Mn_2WO_x/TiO_2-SiO_2(10)$ is somewhat worse than that of the Mn_2WO_x/TiO_2 with the same SHS procedure. Therefore, a modified liquid deposition method is used to prepare the Mn_2WO_x/TiO_2-SiO_2 catalysts later. LPD is a method that through the reaction of the precursors salts solution forms a precipitate and deposit on the solid support pre-placed in the solution to realize the uniform loading of active components. It has been found that $Mn(NO_3)_2$ and $(NH_4)_{10}W_{12}O_{41}$ can not only react to produce a precipitation in the solution, but also form a $MnWO_4$ structure in the precipitation [29], which is considered to be favourable for the activity of Mn_2WO_x/TiO_2 catalysts. Here, the method is also adopted to prepare Mn_2WO_x/TiO_2-SiO_2. The sample exhibits rather high activity in NH_3-SCR reaction. The NO conversion reaches 90% from 200°C to about 400°C, which is even broader than the results of the Mn_2WO_x/TiO_2 by SHS method.

The preparation procedure has a clear influence on the activity of Mn_2WO_x/TiO_2-SiO_2 by LPD method. If the TiO_2-SiO_2 gel was calcined at 500°C before the LPD, the activity of the as-prepared catalyst would decrease. That is to say, the NO conversion only keeps above 90% in a narrow range of 200–230°C. It is because, after calcination, the pore structure of TiO_2-SiO_2 gel is decreased to some extent and the hydrophobicity increases, which is not favourable for the dispersion and deposition of active components. Nonetheless, the LPD method can effectively load $MnWO_x$ active species on the TiO_2-SiO_2 support and keep the activity of Mn_2WO_x/TiO_2-SiO_2 catalyst in the right preparation procedure and conditions.

Figure 2*a* shows the NH_3-SCR activity and figure 2*b* shows the N_2 selectivity of the $Mn_xW_yO_x/TiO_2-SiO_2$ catalysts with different Mn : W ratios synthesized by LPD. It can be seen that the Mn : W ratio influences the temperature window of the $MnWO_x/TiO_2-SiO_2$ catalysts. Taking 90% NO conversion as the criterion, the working temperature window of the $Mn_xW_yO_x/TiO_2-SiO_2$ catalysts varies from 120 to 200°C, 120 to 300°C, 140 to 280°C, 200 to 340°C and 200 to 370°C when the Mn : W ratio decreases from 3 : 1, 2 : 1, 1 : 1, 1 : 2 and 1 : 3, respectively. Taking Mn : W ratio of 1 : 1 as a dividing line, when the manganese content is rich, the catalyst has better activity at low temperatures and worse activity at high temperatures; while when the tungsten is rich, it is just in the opposite way. In general, the Mn_2WO_x/TiO_2-SiO_2 shows the widest working temperature window.

Comparing to activity, Mn : W ratio has a more pronounced effect on N_2 selectivity of the catalyst. In figure 2*b*, over the MnW_2O_x/TiO_2-SiO_2 and MnW_3O_x/TiO_2-SiO_2, the N_2 selectivity is almost unchanged with the temperature rising; while over the other samples, the N_2 selectivity is decreased from about 100% to 87%, 82% and 75% when the Mn : W ratio increases from 1 : 1 to 3 : 1, respectively. The results indicate that Mn element is favourable for the low-temperature activity and W element is favourable for the N_2 selectivity. It is desirable to maintain a certain manganese tungsten ratio for the $MnWO_x/TiO_2-SiO_2$ catalyst to get a satisfying activity and N_2 selectivity.

The support properties often can be adjusted by the composite variation and influence the catalyst properties. TiO_2-SiO_2 oxides with different SiO_2 contents from 5% SiO_2/95% TiO_2 to 20% SiO_2/80%

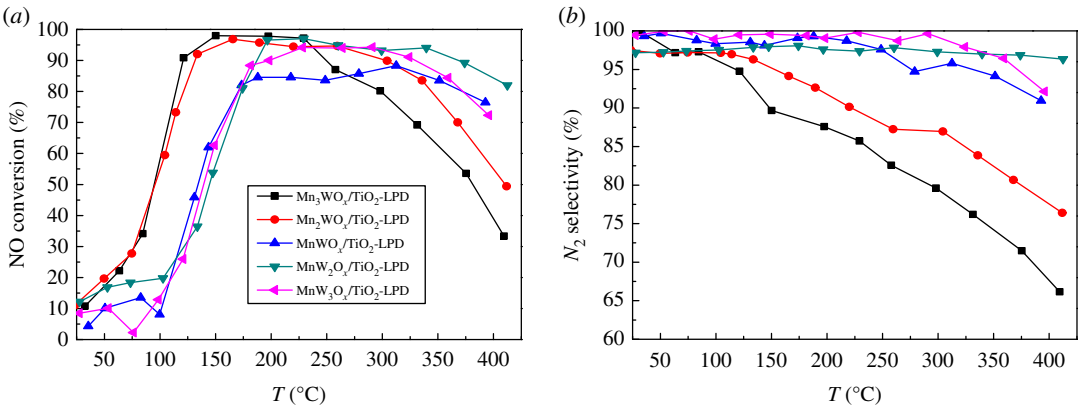

Figure 2. NH_3-SCR activity of $MnWO_x/TiO_2-SiO_2$ with different Mn : W ratios.

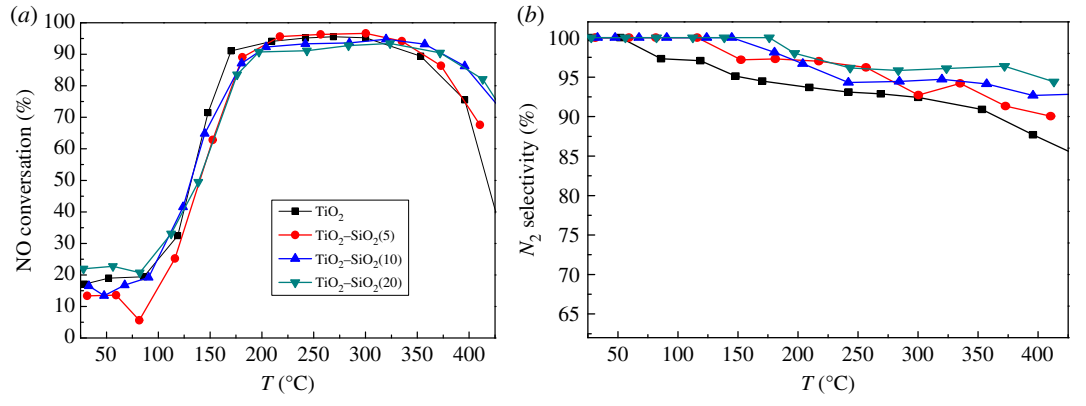

Figure 3. NH_3-SCR activity of $MnWO_x/TiO_2-SiO_2$ with different TiO_2 : SiO_2 per cents.

TiO_2, which are labelled as TiO_2–SiO_2(5), TiO_2–SiO_2(10) and TiO_2–SiO_2(20), are studied. Figure 3*a* shows the results of the activities of the samples in the NH_3-SCR reaction. Taking 90% NO conversion as criterion, the increase of SiO_2 content in the support does not change the working temperature window of Mn_2WO_x/TiO_2–SiO_2 too much. All the low-temperature boundaries of the working temperature windows are around 170°C. When the SiO_2 content increases from 5% to 20%, it only makes the high-temperature boundary move a slight degree to the high-temperature direction, and slightly widens the working temperature window. The working temperature windows of Mn_2WO_x/TiO_2–SiO_2(10) and Mn_2WO_x/TiO_2–SiO_2(20) are the same as 170–370°C.

The addition of SiO_2 also has a positive effect on the N_2 selectivity of the catalyst, as shown in figure 3*b*. It can be found that N_2 selectivity on the Mn_2WO_x/TiO_2 (without SiO_2) catalyst at 50°C began to decrease rapidly with the increase of temperature. Nonetheless, the N_2 selectivity can be maintained at above 90% on all the Mn_2WO_x/TiO_2–SiO_2 samples. Further, as the SiO_2 content increases, N_2 selectivity decreases slowly, and it decreases the slowest on the Mn_2WO_x/TiO_2–SiO_2(20) sample.

3.2. The resistance of $MnWO_x/TiO_2-SiO_2$ to H_2O and SO_2

As is known, the flue gas usually contains SO_2 and water vapour, which often affects the NH_3-SCR catalyst performance. It is the primary reason that the Mn_2WO_x/TiO_2 catalyst is modified by SiO_2 in this paper. Figure 4 shows the NH_3-SCR results of Mn_2WO_x/TiO_2–SiO_2 catalysts with different SiO_2 content in 100 ppm SO_2 at different reaction temperature. The SO_2 is introduced after 60 min of reaction time on stream.

It can be seen that SiO_2 has a significant effect on the sulfur resistance of the Mn_2WO_x/TiO_2–SiO_2 catalyst. Taking the introduction time of SO_2 flow (60 min) as the initial point, for the Mn_2WO_x/TiO_2 catalyst, the NO conversion begins to decrease after 90 min (total 150 min time on stream) reaction after the introduction of SO_2 flow. It decreases with a slow rate till 240 min (total 300 min), and then

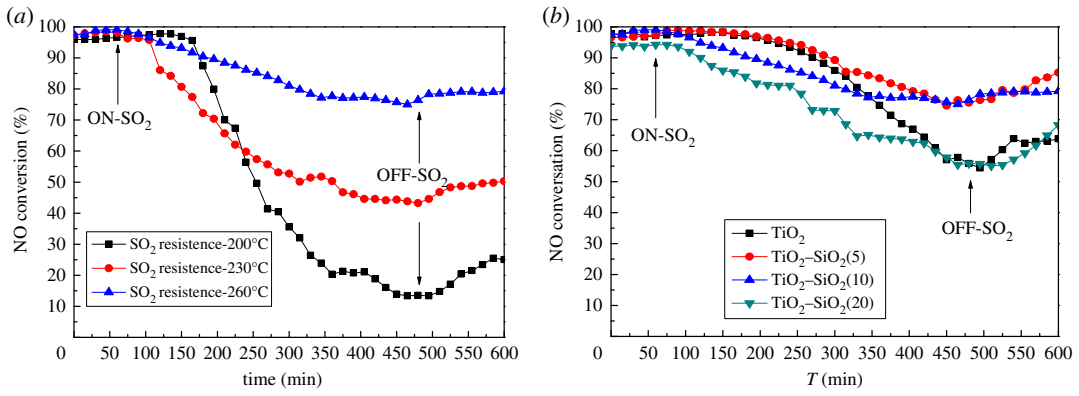

Figure 4. NH_3-SCR activity of Mn_2WO_x/TiO_2-SiO_2 in 100 ppm SO_2.

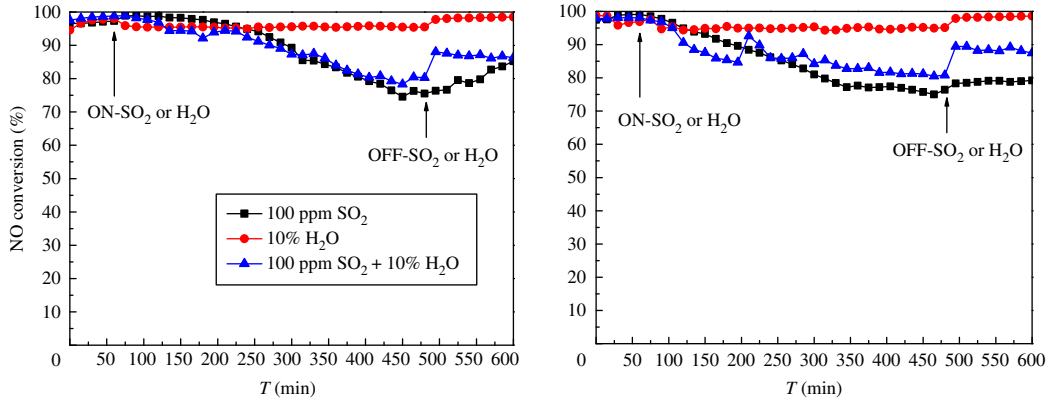

Figure 5. NH_3-SCR activity of $Mn_2WO_x/TiO_2-SiO_2(5)$ and $Mn_2WO_x/TiO_2-SiO_2(10)$ at 260°C in the presence of H_2O, SO_2 and $SO_2 + H_2O$.

decreases with a significant rate to 55% at 420 min (total 480 min), where SO_2 is switched off. The NO conversion then rises back to about 65% in SO_2-free flow after 120 min (total 600 min on stream). The performance of $Mn_2WO_x/TiO_2-SiO_2(5)$ was similar to that of Mn_2WO_x/TiO_2 catalyst before 240 min, but the NO conversion decreased significantly slower than the Mn_2WO_x/TiO_2 catalyst. The NO conversion is still close to 80% at 420 min, and after SO_2 switches off for 120 min, it rises back to close to 90% again. For the catalyst $Mn_2WO_x/TiO_2-SiO_2(10)$, the NO conversion decreases with a rather slow rate after 30 min of SO_2 flow introduction in a linear style till 300 min, where the NO conversion is kept at about 80%. In the remaining time, no significant change is observed even though the SO_2 is switched off. Finally, for the catalyst $Mn_2WO_x/TiO_2-SiO_2(20)$, the NO conversion decreases clearly in a different way from other samples. A number of stable platforms appeared on the profile, mainly in the range of 160–220 min, 260–300 min and 330–420 min total time on stream. When the SO_2 is switched off, the NO conversion can rise back to about 70% after 120 min. The results show that the appropriate amount of SiO_2 is beneficial to improve the sulfur resistance of the Mn_2WO_x/TiO_2-SiO_2 catalyst.

To further evaluate the effect, the performance of $Mn_2WO_x/TiO_2-SiO_2(10)$ is then tested under 230°C and 200°C. However, the results in figure 4*b* are not very good. At 230°C, NO conversion has dropped below 50% after 420 min on stream; and at 200°C, NO conversion only is left no more than 20%. It means that the effect of SiO_2 is still limited and the catalyst needs to be more improved in the future.

Next, the activity of $Mn_2WO_x/TiO_2-SiO_2(5)$ and Mn_2WO_x/TiO_2-SiO_2 (10) at 260°C in the presence of 10% H_2O and $SO_2 + H_2O$ together are investigated in figure 5. Both of the NO conversions can maintain above 95% in the presence of 10% H_2O. After the H_2O is switched off, the activity of the catalyst can be fully restored in a short time, indicating that the catalyst has good resistance to H_2O. In the 10 vol% H_2O and 100 ppm SO_2 atmosphere, the NO conversion profile on the $Mn_2WO_x/TiO_2-SiO_2(5)$ is similar with that in the 100 ppm SO_2 flow, while its decrease degree is a little slight. The NO conversion is kept above 80% at 480 min. When H_2O and SO_2 are stopped, NO conversion rate rises rapidly. As for the $Mn_2WO_x/TiO_2-SiO_2(10)$, the NO conversion quickly decreases to about

Table 1. The texture properties of different catalysts and supports before reaction.

samples	BET surface area ($m^2\ g^{-1}$)	average pore diameter (nm)	pore volume ($cm^3\ g^{-1}$)
$Mn_2WO_x/TiO_2-SiO_2(20)$	219.5	2.7	0.150
$Mn_2WO_x/TiO_2-SiO_2(10)$	219.6	2.6	0.142
$Mn_2WO_x/TiO_2-SiO_2(5)$	235.9	2.9	0.170
Mn_2WO_x/TiO_2	184.1	2.9	0.135
$TiO_2-SiO_2(20)$	332.6	2.6	0.213
$TiO_2-SiO_2(10)$	283.5	2.2	0.158
$TiO_2-SiO_2(5)$	263.9	2.2	0.145
TiO_2	215.7	2.2	0.120

Table 2. The texture properties of different catalysts after reactions.

samples	BET surface area ($m^2\ g^{-1}$)	average pore diameter (nm)	pore volume ($cm^3\ g^{-1}$)
$Mn_2WO_x/TiO_2-SiO_2(20)-SO_2$	147.7	2.8	0.104
$Mn_2WO_x/TiO_2-SiO_2(20)-H_2O$	208.7	2.7	0.143
$Mn_2WO_x/TiO_2-SiO_2(20)-SO_2+H_2O$	140.5	2.8	0.099
$Mn_2WO_x/TiO_2-SiO_2(10)-SO_2$	177.2	2.7	0.120
$Mn_2WO_x/TiO_2-SiO_2(10)-H_2O$	210.2	2.6	0.136
$Mn_2WO_x/TiO_2-SiO_2(10)-SO_2+H_2O$	167.8	2.6	0.109
$Mn_2WO_x/TiO_2-SiO_2(5)-SO_2$	187.9	2.7	0.129
$Mn_2WO_x/TiO_2-SiO_2(5)-H_2O$	221.4	2.9	0.161
$Mn_2WO_x/TiO_2-SiO_2(5)-SO_2+H_2O$	168.6	2.8	0.118
Mn_2WO_x/TiO_2-SO_2	125.2	3.1	0.096
Mn_2WO_x/TiO_2-H_2O	174.3	2.9	0.124
$Mn_2WO_x/TiO_2-SO_2+H_2O$	116.5	3.1	0.087

80% and keeps at that level till 480 min. When the H_2O and SO_2 is switched off, it also rises back to about 90% in a short time. That is to say, both of the samples show good resistance to the H_2O and SO_2.

3.3. Catalysts characterization

Table 1 lists some texture properties such as the specific surface area, the average pore size and pore volume of the TiO_2–SiO_2 supports and the Mn_2WO_x/TiO_2–SiO_2 catalysts prepared by sol–gel method and LPD. It can be found that the addition of SiO_2 clearly increases the specific surface area of TiO_2–SiO_2 gels comparing to TiO_2. With the increase of SiO_2 amount, the specific surface area of TiO_2–$SiO_2(5)$, TiO_2–$SiO_2(10)$ and TiO_2–$SiO_2(20)$ increases from 263.9 and 283.5 to 332.6 $m^2\ g^{-1}$; the pore volume increases from 0.145 and 0.158 to 0.213 $cm^3\ g^{-1}$, respectively. While the average pore size is kept at about 2.2 nm, only TiO_2–$SiO_2(20)$ is increased to 2.6 nm. When the active species are loaded on the TiO_2–SiO_2 support, all the specific surface areas and pore volumes of Mn_2WO_x/TiO_2–SiO_2 catalysts are decreased, while the average pore sizes are increased. The Mn_2WO_x/TiO_2–$SiO_2(5)$ catalyst can be found to have the best pore structure and keep the largest specific surface area of 235.9 $m^2\ g^{-1}$, the average pore diameter of 2.9 nm and pore volume of 0.170 $cm^3\ g^{-1}$.

The texture properties of the heterogenous catalyst are often changed after the reaction. To investigate the properties of Mn_2WO_x/TiO_2–SiO_2 catalysts before and after the NH_3-SCR reaction in the different atmospheres, table 2 lists their texture properties after the NH_3-SCR reaction with/without H_2O and SO_2 flow.

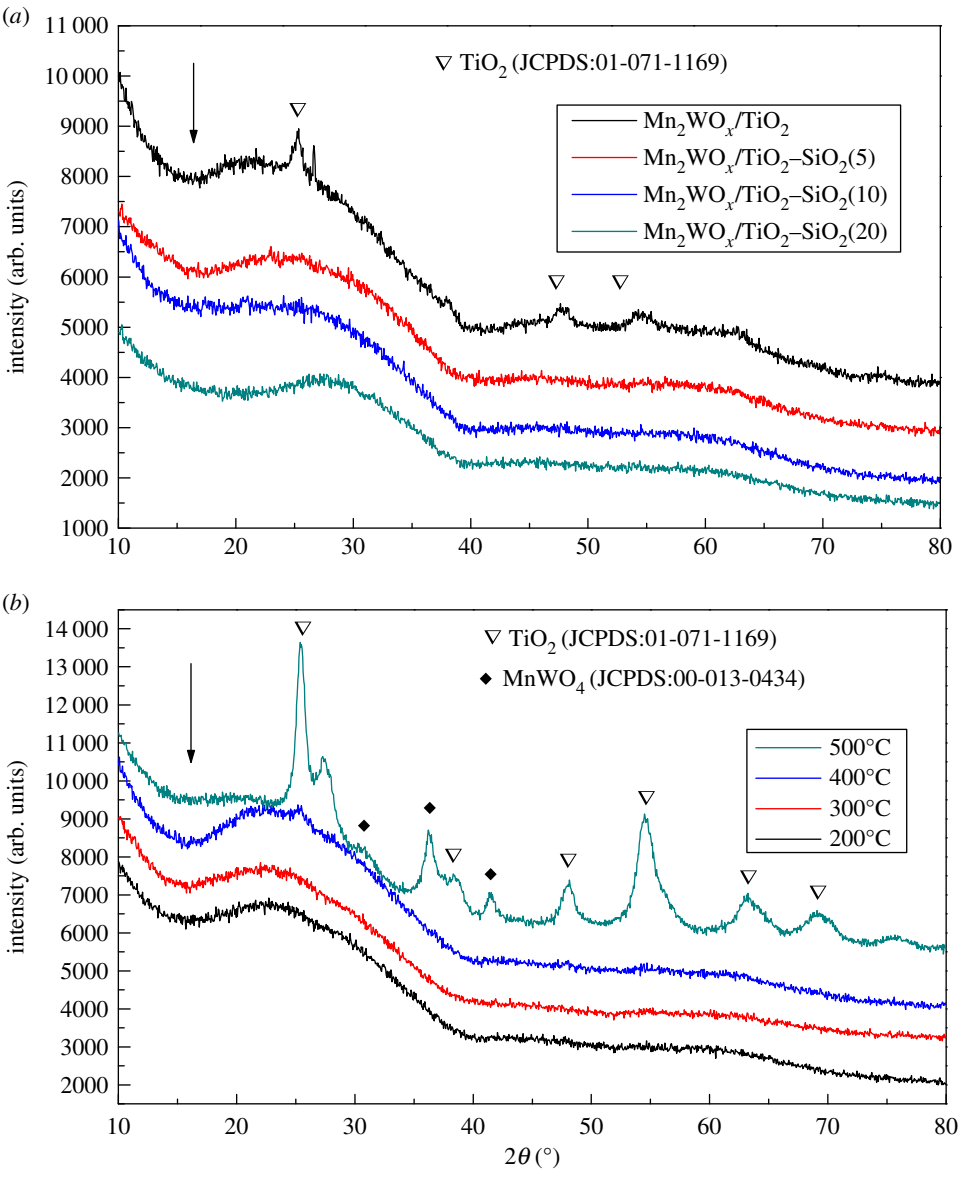

Figure 6. XRD patterns of Mn_2WO_x/TiO_2-SiO_2 catalysts.

The presence of water has little effect on the texture properties of the catalysts. All the average pore sizes do not change after reaction, and the specific surface area of the catalysts decreases about 10 $m^2\,g^{-1}$. SO_2 significantly affects the nature of the catalysts. All the specific surface area and pore volumes of the catalysts after the reaction are largely reduced. The largest decrement is from Mn_2WO_x/TiO_2–SiO_2(20). The specific surface area decreases 71.8 $m^2\,g^{-1}$, and the pore volume decreases 0.046 $cm^3\,g^{-1}$. The second is the Mn_2WO_x/TiO_2, 67.3 $m^2\,g^{-1}$ and 0.048 $cm^3\,g^{-1}$. Mn_2WO_x/TiO_2–SiO_2(10) and Mn_2WO_x/TiO_2–SiO_2(5) show somewhat better resistance to SO_2. Their specific surface areas only decrease 42.4 and 48 $m^2\,g^{-1}$. Especially, the pore volume of Mn_2WO_x/TiO_2–SiO_2(10) only decreases 0.022 $cm^3\,g^{-1}$. The average pore size of Mn_2WO_x/TiO_2–SiO_2(5) sample is the only one enlarged after the reaction. Coexistence of water and SO_2 does not show a synergistic effect on the nature of the catalysts. The change in the values is close to the sum of the influence of the two compounds.

Figure 6 shows the XRD pattern of the Mn_2WO_x/TiO_2–SiO_2 catalysts. It can be seen that for the as-prepared Mn_2WO_x/TiO_2–SiO_2 catalysts, except the profile of Mn_2WO_x/TiO_2 sample shows the characteristics peaks of $2\theta = 25.2°$, 48.1°, 54.0° and 62.8° attributed to the anatase TiO_2, neither the characteristic peaks of active species such as MnO_x, WO_3 and $MnWO_x$, nor the characteristic peaks of support such as the anatase TiO_2 and rutile TiO_2 or SiO_2 appear on the other samples. The results may indicate the uniformity of the crystal sizes of the support and active species carrier are

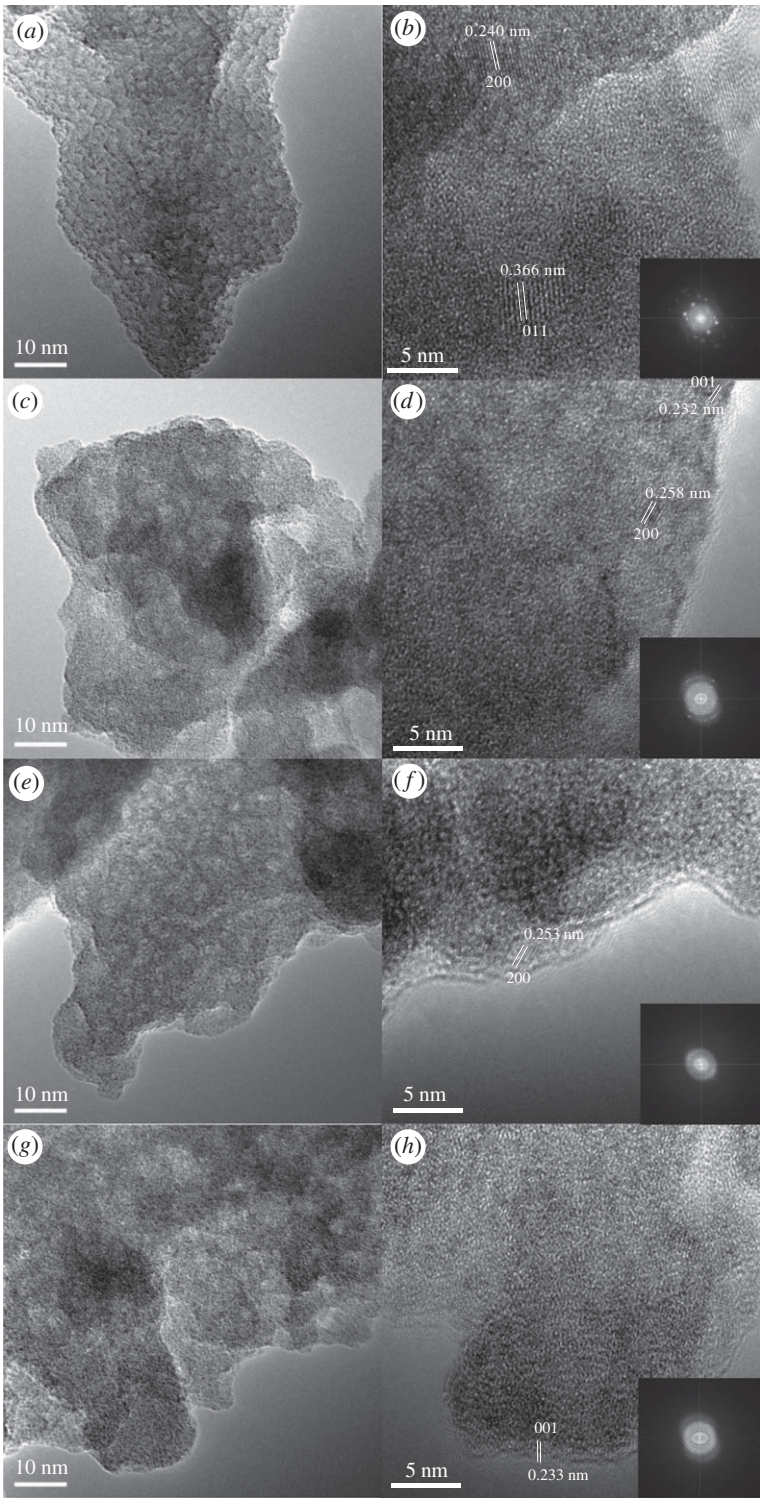

Figure 7. TEM images of the Mn_2WO_x/TiO_2-SiO_2 catalysts. (*a*,*b*) Mn_2WO_x/TiO_2, (*c*,*d*) $Mn_2WO_x/TiO_2-SiO_2(5)$, (*e*,*f*) $Mn_2WO_x/TiO_2-SiO_2(10)$, (*g*,*h*) Mn_2WO_x/TiO_2 -$SiO_2(20)$.

uniform and small, but it may also mean that the resulting catalysts are predominantly the amorphous species.

Figure 7 then exhibits the morphologies of the catalysts by TEM. From the images, on the surface of the silicon-free Mn_2WO_x/TiO_2, there are clear crystal lattice fringes, which can be identified and attributed to the different crystal faces of the active species or the supports. The 0.345 nm lattice spacing is from (101) face of TiO_2; 0.240 nm and 0.366 nm spacing can be attributed to with (200) and (011) face of $MnWO_4$ crystal. It is similar to our previous results obtained by SHS method [22]. The

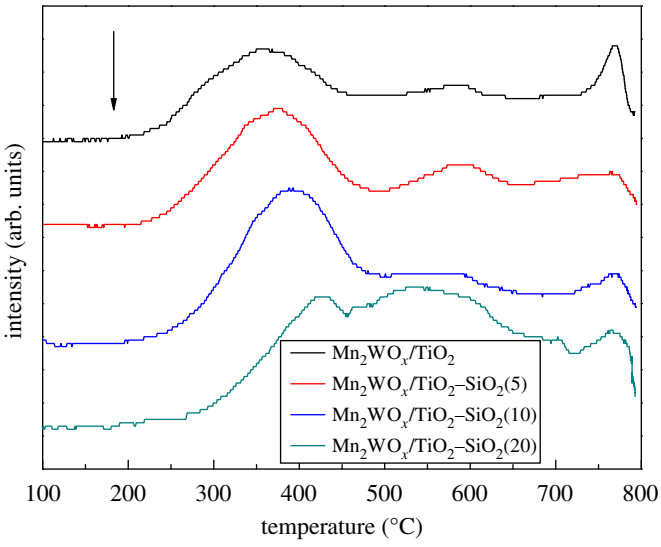

Figure 8. H_2-TPR profiles of the Mn_2WO_x/TiO_2-SiO_2 catalysts.

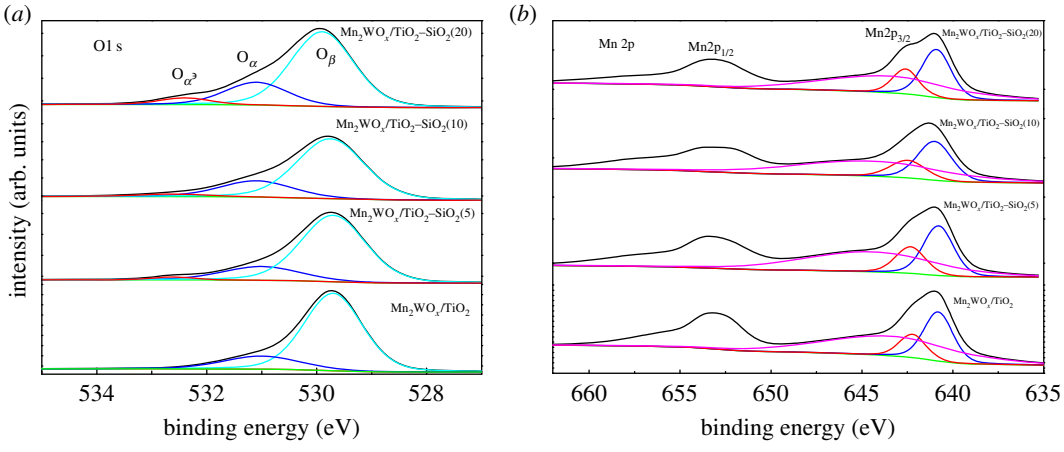

Figure 9. O1 s (*a*) and Mn 2p (*b*) XPS spectra of the Mn_2WO_x/TiO_2-SiO_2 catalysts.

results confirmed that the reaction to form manganese tungstate has occurred in the solution. The sample has well crystallinity with a uniform particles size distribution. Meanwhile, for the silicon-containing samples, the particles are also relatively small. But the lattice fringes are not very clear due to the high contents of the mixed crystal composition, which means that the SiO_2 affects the crystallinity of the $MnWO_x$ active species.

Figure 8 shows the H_2-TPR profiles of $Mn_2WO_x/TiO_2–SiO_2$ catalysts with different SiO_2 contents. The reduction peaks may originate from the different active species and supports, which leads to the profiles somewhat complicated. In general, the profile can be divided into two reduction bands and one big peak. According to the previous discussions [30–32], for the Mn_2WO_x/TiO_2 sample, in the lower temperature range of 250–480°C, the reduction bands or peaks are mainly originated from different MnO_x species; in the higher temperature range of 500–800°C, the reduction band and peak are from different Ti or W oxides species. More detailed, the identified reduction peaks at about 300°C and 340°C are attributed to the reduction peaks of $MnO_2 \rightarrow Mn_3O_4$ and $Mn_3O_4 \rightarrow MnO$. The reduction band of 520°C–600°C is the contribution of $Ti^{4+} \rightarrow Ti^{3+}$, and the peak at 780°C is from $W^{6+} \rightarrow W^{4+}$. When the SiO_2 is introduced into TiO_2, there are several significant changes observed. The first is that the reduction band in the low-temperature range moves to the high-temperature attitude; the second is the strength of the reduction band in the middle temperature increases and the peak at 780°C decreases. The movement of the band in the low-temperature range means that the MnO_x species are inclined to be hard to reduce, which shall not be favourable for the NH_3-SCR activity of the $Mn_2WO_x/TiO_2–SiO_2$ catalysts. However, the NH_3-SCR activity seems to be not influenced clearly. It might be amended by the dispersion increment of active species by the $TiO_2–SiO_2$ support. The

Table 3. Quantitative results of O1 s XPS spectra of Mn_2WO_x/TiO_2-SiO_2 (0–20%).

	O_β		O_α		$O_{\alpha'}$	
samples	BE (eV)	Per. (%)	BE (eV)	Per. (%)	BE (eV)	Per. (%)
Mn_2WO_x/TiO_2	529.7	81.67	531.0	18.32	532.6	0
$Mn_2WO_x/TiO_2-SiO_2(5)$	529.7	78.40	531.0	19.47	532.6	2.13
$Mn_2WO_x/TiO_2-SiO_2(10)$	529.7	74.82	531.1	21.84	532.6	3.34
$Mn_2WO_x/TiO_2-SiO_2(20)$	529.9	72.60	531.1	22.20	532.4	5.21

Table 4. Quantitative results of Mn2p XPS spectra of Mn_2WO_x/TiO_2-SiO_2 (0–20%).

	Mn^{4+}		Mn^{3+}		Mn^{2+}		
samples	BE (eV)	Per. (%)	BE (eV)	Per. (%)	BE (eV)	Per. (%)	Average valence
Mn_2WO_x/TiO_2	642.2	13.33	640.8	30.55	643.4	56.11	2.6
$Mn_2WO_x/TiO_2-SiO_2(5)$	642.3	15.86	640.8	30.24	644.5	53.89	2.6
$Mn_2WO_x/TiO_2-SiO_2(10)$	642.5	14.68	641.0	31.42	644.5	53.89	2.6
$Mn_2WO_x/TiO_2-SiO_2(20)$	642.6	15.08	640.9	32.89	643.5	51.93	2.6

strength increment of the peak at the middle temperature illustrates that more TiO_2 can be reduced. The TiO_2 crystal structure might be broken and more amorphous or isolated species have been formed.

In order to investigate the valence state of the Mn species and O species, XPS characterization was performed for the samples. Figure 9*a* shows the O1 s spectra of Mn_2WO_x/TiO_2, Mn_2WO_x/TiO_2–$SiO_2(5)$, Mn_2WO_x/TiO_2–$SiO_2(10)$ and Mn_2WO_x/TiO_2–$SiO_2(20)$, and table 3 lists the quantitative results via Gauss deconvolution method. After deconvolution, three sub-bands can be found on the spectra. As previous reports, the sub-bands around 529.7 eV can be attributed to the lattice oxygen (denoted as O_β); the sub-bands around 531.1 eV to surface absorbed oxygen (denoted as O_α) such as O_2^{2-} and O^-, and the sub-band around 533.2 eV can be assigned to chemisorbed water (denoted as $O_{\alpha'}$) [17,33]. With the SiO_2 introduction increases, the peak of O_β decreases and the peak of O_α and $O_{\alpha'}$ increases gradually. As the O_α is usually regarded as more reactive in redox reactions due to its higher mobility than lattice oxygen, the percentages of O_α, O_β and $O_{\alpha'}$ are often viewed as an indicator for the redox ability of the catalyst. From table 3, the O_α per cent increases gradually from 18.32% of the Mn_2WO_x/TiO_2 to 22.20% of Mn_2WO_x/TiO_2–$SiO_2(20)$. Combining the results of XRD and TEM, it may infer that the addition of SiO_2 decreases the crystallinity of the active species, increases the dispersion, and forms more surface active sites. Some reports mentioned that the sub-band around 529.7 eV could be attributed to Ti–O–Ti bonds; the sub-band around 532.1 eV to Si–O–Ti cross-linking bonds, and the sub-band around 533.2 eV to Si–O–Si bonds [34,35]. When the SiO_2 introduction increases, the peak of Ti–O–Ti bonds decreases and the peak of Si–O–Ti cross-linking bonds and Si–O–Si bonds increases gradually.

Figure 9*b* then shows the Mn 2p XPS spectra of the four samples and table 4 lists the quantitative results. Similarly, three sub-bands belonging to Mn^{3+} at 640.6–641.4 eV, Mn^{4+} at 641.9–642.3 eV and Mn^{2+} at 643.4–644.5 eV can be found on the spectra. According to the quantitative analysis, the Mn species with different valence states does not change clearly, and the average valence state does not change, which may indicate that the SiO_2 only improves the dispersion of the active species, and has not much interaction effect with the active species after loading.

At the same time, $O_{\alpha'}$ increment means that the introduction of SiO_2 increases the adsorption of water on the Mn_2WO_x/TiO_2–SiO_2. Thus, it seems that the hydrophobicity of Mn_2WO_x/TiO_2–SiO_2 is decreased, which shall be not favourable for the water resistance and the activity. While the above activity experiments have demonstrated that the water resistance of the catalyst is enhanced, to explain the phenomenon, the water adsorption ability of the catalysts are measured under different temperatures. The results are listed in table 5. From the results, the water adsorption capacity of the Mn_2WO_x/TiO_2–SiO_2 samples are lower than the Mn_2WO_x/TiO_2 at room temperature (RT) and decreased with the SiO_2 content. Further, the difference is more pronounced at high temperature (100°C).

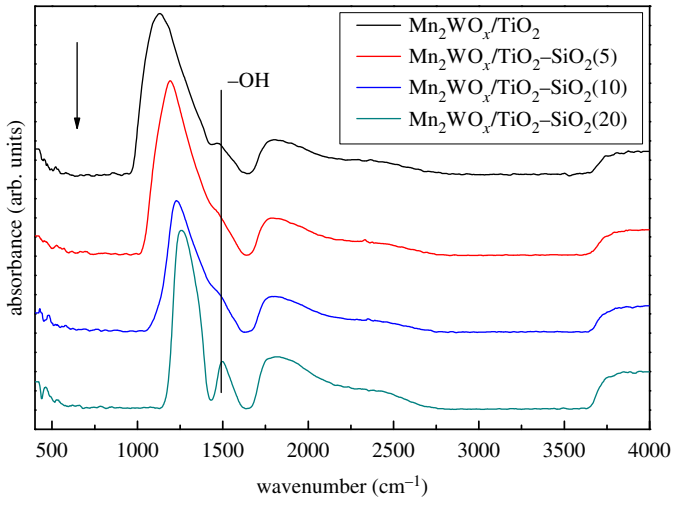

Figure 10. Skeleton FT-IR of the Mn_2WO_x/TiO_2-SiO_2 catalysts.

Table 5. The hydrophobicity of catalysts under different temperature.

samples	dry basis (g)	saturated with water at RT (g)	saturated with water at 100°C (g)	water adsorption capacity at RT (g g^{-1})	water adsorption capacity at 100°C (g g^{-1})
Mn_2WO_x/TiO_2	0.5408	0.6081	0.5772	0.1244	0.0673
$Mn_2WO_x/TiO_2-SiO_2(5)$	0.5129	0.5755	0.5426	0.1221	0.0579
$Mn_2WO_x/TiO_2-SiO_2(10)$	0.4928	0.5450	0.5143	0.1059	0.0436
$Mn_2WO_x/TiO_2-SiO_2(20)$	0.6055	0.6650	0.6262	0.0983	0.0342

The weak water adsorption capacity of the Mn_2WO_x/TiO_2-SiO_2 catalysts may come from the formation of silicon hydroxyl. The skeleton FT-IR of the Mn_2WO_x/TiO_2-SiO_2 catalysts is then recorded and the results are shown in figure 10. It can be found that the hydroxyl vibration peaks at 1502 cm^{-1} are significantly changed after introduction of SiO_2. For the $Mn_2WO_x/TiO_2-SiO_2(20)$, it has changed from the shoulder peak to the independent peak, corresponding to its higher water adsorption. Meanwhile, the peak is weakened for the $Mn_2WO_x/TiO_2-SiO_2(5)$ and the $Mn_2WO_x/TiO_2-SiO_2(10)$ and their water adsorption content are somewhat lower too. Thus, the appropriate SiO_2 content can reduce the amount of hydroxyl groups on the catalyst surface, and the excessive SiO_2 increases the amount of hydroxyl groups on the catalyst surface.

3.4. Discussions

As mentioned earlier, this paper is intended to indirectly improve the SO_2 resistance of the $MnWO_x/TiO_2$ catalyst by increasing its hydrophobicity. According to the activity tests, the SO_2 and water resistance of the $MnWO_x/TiO_2-SiO_2$ catalyst can be really improved under the premise that the NH_3-SCR activity is maintained. The NO conversion is no longer decreased as soon as the catalyst contacts SO_2, but it is maintained for some time on stream and then decreased slowly. Meanwhile, the water adsorption test shows that the water capacity of the catalyst decreases after SiO_2 introduction.

However, it is a little hasty to make this assertion, as SiO_2 introduction also changes some other properties of the catalyst. The specific surface area and pore volume of the $MnWO_x/TiO_2-SiO_2$ catalysts is clearly larger than the $MnWO_x/TiO_2$. The decreasing degree of the specific surface area and pore volume of the $MnWO_x/TiO_2-SiO_2$ catalysts after reaction is also lighter than the $MnWO_x/TiO_2$. Therefore, TG analysis has been performed after reaction and the results are displayed in

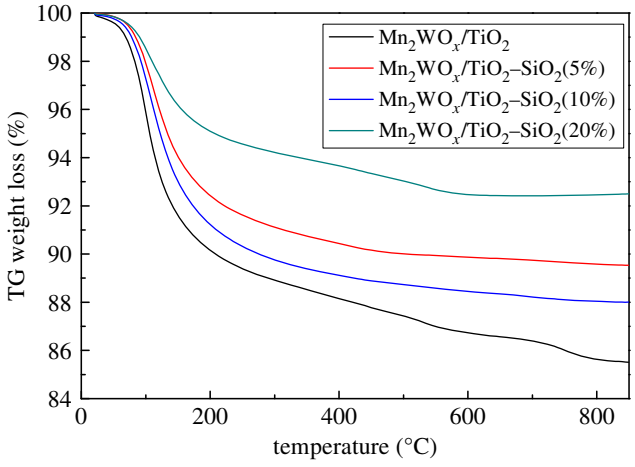

Figure 11. TG results of different $Mn_2WO_x/TiO_2–SiO_2$ catalysts after 600 min reaction.

figure 11. From the TG results, the water adsorption capacity of the $Mn_2WO_x/TiO_2–SiO_2$ catalysts is clearly lower than that of the Mn_2WO_x/TiO_2. The weight loss of the $Mn_2WO_x/TiO_2–SiO_2(5)$ and $Mn_2WO_x/TiO_2–SiO_2(10)$ catalysts in higher temperature are also significantly lower than that of the Mn_2WO_x/TiO_2. It may be helpful to prove that both the coke behaviour and hydrophobicity are restrained after SiO_2 doping.

4. Conclusion

A series of $TiO_2–SiO_2$ mixed oxides supports were prepared by sol–gel method, and the $MnWO_x$ active components were loaded on the supports by liquid deposition method to form a series of $MnWO_x/TiO_2–SiO_2$ catalysts. Owing to the reaction of manganese nitrate and ammonia tungstate to form $MnWO_4$, the catalysts could be prepared at low temperature. The introduction of SiO_2 in the TiO_2 support increases the N_2 selectivity of the $MnWO_x/TiO_2$ catalyst without decreasing the NH_3-SCR activity. Meanwhile, with appropriate SiO_2 (5% and 10% percentage of TiO_2), the sulfur resistance of $MnWO_x/TiO_2–SiO_2$ is clearly improved, the decreasing rate and degree of NO conversion are both slowed down and retarded. By a series of BET, XRD and TEM characterization, it can be inferred that the texture properties of $MnWO_x/TiO_2–SiO_2$ are modified and the dispersion of $MnWO_x$ species is improved, which is beneficial for the NH_3-SCR activity. Skeleton FT-IR, water adsorption capacity and XPS show that SiO_2 introduction decreases the water adsorption capacity especially at the high temperatures, which might be favourable for the water and sulfur resistance of the catalyst.

Data accessibility. Our data are available from Dryad Digital Repository: doi:10.5061/dryad.74pj317 [36].

Authors' contributions. W.Z.L. carried out the molecular laboratory work, participated in data analysis, carried out sequence alignments; Z.K.Z. participated in the design of the study and drafted the manuscript; H.F.L. conceived of the study, designed the study, coordinated the study and helped draft the manuscript. All authors gave final approval for publication.

Competing interests. We have no competing interests.

Funding. This work is supported by the Natural Science Foundation of China (grant nos. 21506194 and 21676255).

References

1. Granger P. 2017 Challenges and breakthroughs in postcombustion catalysis: how to match future stringent regulations. *Catal. Sci. Technol.* **7**, 5195–5211. (doi:10.1039/C7CY00983F)
2. Beale AM, Gao F, Lezcano-Gonzalez I, Pedenc CHF, Szanyi J. 2015 Recent advances in automotive catalysis for NO_x emission control by small-pore microporous materials. *Chem. Soc. Rev.* **44**, 7371–7405. (doi:10.1039/C5CS00108K)
3. Lei TY, Li QC, Chen SF, Liu ZY, Liu QY. 2016 KCl-induced deactivation of V_2O_5-WO_3/TiO_2 catalyst during selective catalytic reduction of NO by NH_3: comparison of poisoning methods. *Chem. Eng. J.* **296**, 1–10. (doi:10.1016/j.cej.2016.03.095)
4. He YY, Ford ME, Zhu MH, Liu QC, Tumuluri U, Wu ZL, Wachs IE. 2016 Influence of catalyst synthesis method on selective catalytic reduction (SCR) of NO by NH_3 with V_2O_5-WO_3/TiO_2 catalysts. *Appl. Catal. B: Environ.* **193**, 141–150. (doi:10.1016/j.apcatb.2016.04.022)
5. Wang C, Yang SJ, Chang HZ, Peng Y, Li JH. 2013 Dispersion of tungsten oxide on SCR performance of V_2O_5-WO_3/TiO_2: acidity, surface species and catalytic activity. *Chem. Eng. J.* **225**, 520–527. (doi:10.1016/j.cej.2013.04.005)
6. Tang CJ, Zhang HL, Dong L. 2016 Ceria-based catalysts for low-temperature selective catalytic

reduction of NO with NH_3. *Catal. Sci. Technol.* **6**, 1248–1264. (doi:10.1039/C5CY01487E)

7. Yan LJ, Liu YY, Zha KW, Li HR, Shi LY, Zhang DS. 2017 Scale–activity relationship of MnO_x-FeO_y nanocage catalysts derived from Prussian blue analogues for low-temperature NO reduction: experimental and DFT studies. *ACS Appl. Mater. Inter.* **9**, 2581–2593. (doi:10.1021/acsami.6b15527)
8. Zha KW, Cai SX, Hu H, Li HR, Yan TT, Shi LY, Zhang DS. 2017 In situ DRIFTs investigation of promotional effects of tungsten on MnO_x-CeO_2/meso-TiO_2 catalysts for NO_x reduction. *J. Phys. Chem. C* **121**, 25 243–25 254. (doi:10.1021/acs.jpcc.7b08600)
9. Zha KW, Kang L, Feng C, Han LP, Li HR, Yan TT, Maitarad P, Shi LY, Zhang DS. 2018 Hollandite Mn–Ti oxide promoted Cu-SAPO-34 catalysts exhibited outstanding deNOx performance and excellent resistance against alkali metal poisoning. *Environ. Sci. Nano* **5**, 1408–1419. (doi:10.1039/C8EN00226F)
10. Hu XN, Huang L, Zhang JP, Li HR, Zha KW, Shi LY, Zhang DS. 2018 Facile and template-free fabrication of mesoporous 3D nanosphere-like $Mn_xCo_{3-x}O_4$ as highly effective catalysts for low temperature SCR of NO_x with NH_3. *J. Mater. Chem. A* **6**, 2952–2963. (doi:10.1039/C7TA08000J)
11. Li CL, Tang XX, Yi HH, Wang LF, Cui XX, Chu C, Li JY, Zhang R, Yu QJ. 2018 Rational design of template-free MnO_x-CeO_2 hollow nanotube as de-NOx catalyst at low temperature. *Appl. Surf. Sci.* **428**, 924–932. (doi:10.1016/j.apsusc.2017.09.131)
12. Yang SJ, Qi FH, Xiong SC, Dang H, Liao Y, Wong PK, Li JH. 2016 MnOx supported on Fe–Ti spinel: A novel Mn based low temperature SCR catalyst with a high N_2 selectivity. *Appl. Catal. B: Environ.* **181**, 570–580. (doi:10.1016/j.apcatb.2015.08.023)
13. Liu C, Shi JW, Gao C, Niu CM. 2016 Manganese oxide-based catalysts for low-temperature selective catalytic reduction of NO_x with NH_3: a review. *Appl. Catal. A: Gen.* **522**, 54–69. (doi:10.1016/j.apcata.2016.04.023)
14. Li X, Li JH, Peng Y, Chang HZ, Zhang T, Zhao S, Si WZ, Hao JM. 2016 Mechanism of arsenic poisoning on SCR catalyst of CeW/Ti and its novel efficient regeneration method with hydrogen. *Appl. Catal. B: Environ.* **184**, 246–257. (doi:10.1016/j.apcatb.2015.11.042)
15. Zhang T, Qu RY, Su WK, Li JH. 2015 A novel Ce–Ta mixed oxide catalyst for the selective catalytic reduction of NO_x with NH_3. *Appl. Catal. B: Environ.* **176–177**, 338–346. (doi:10.1016/j.apcatb.2015.04.023)
16. Ding SP, Liu FD, Shi XY, He H. 2016 Promotional effect of Nb additive on the activity and hydrothermal stability for the selective catalytic reduction of NO_x with NH_3 over CeZrOx catalyst. *Appl. Catal. B: Environ.* **180**, 766–774. (doi:10.1016/j.apcatb.2015.06.055)
17. Shan WP, Liu FD, He H, Shi XY, Zhang CB. 2012 A superior Ce-W-Ti mixed oxide catalyst for the selective catalytic reduction of NO_x with NH_3. *Appl. Catal. B: Environ.* **115–116**, 100–106. (doi:10.1016/j.apcatb.2011.12.019)
18. Zhan SH, Zhang H, Zhang Y, Shi Q, Li Y, Li XJ. 2017 Efficient NH_3-SCR removal of NO_x with highly ordered mesoporous $WO_3(\chi)$-CeO_2 at low temperatures. *Appl. Catal. B: Environ.* **203**, 199–209. (doi:10.1016/j.apcatb.2016.10.010)
19. Woolfolk LG, Geantet C, Massin L, Laurenti D, Reyesa JAD. 2017 Solvent effect over the promoter addition for a supported NiWS hydrotreating catalyst. *Appl. Catal. B: Environ.* **201**, 331–338. (doi:10.1016/j.apcatb.2016.07.052)
20. Liu FD, Shan WP, Lian ZH, Xie LJ, Yang WW, He H. 2013 Novel $MnWO_x$ catalyst with remarkable performance for low temperature NH_3-SCR of NO_x. *Catal. Sci. Technol.* **3**, 2699–2707. (doi:10.1039/C3CY00326D)
21. Sun WB, Li XY, Zhao QD, Tade M, Liu SM. 2015 WαMn1 − αOx catalysts synthesized by a one-step urea co-precipitation method for selective catalytic reduction of NO_x with NH_3 at low temperatures. *Energy Fuels.* **30**, 1810–1814. (doi:10.1021/acs.energyfuels.5b02252)
22. Kong ZJ, Wang C, Ding ZN, Chen YF, Zhang ZK. 2015 Enhanced activity of MnxW0.05Ti0.95-xO2-δ for selective catalytic reduction of NO_x with ammonia by self-propagating high-temperature synthesis. *Catal. Commun.* **64**, 27–31. (doi:10.1016/j.catcom.2015.01.028)
23. Lu P, Li H, Liu HY, Chen CY, Zhang ZK. 2018 Influence of tungsten on the NH_3-SCR activity of $MnWO_x/TiO_2$ catalysts. *RSC Adv.* **7**, 19 771–19 779. (doi:10.1039/C7RA00427C)
24. Yu J, Guo F, Wang YL, Zhu JH, Liu YY, Su FB, Gao SQ, Xu GW. 2010 Sulfur poisoning resistant mesoporous Mn-base catalyst for low-temperature SCR of NO with NH_3. *Appl. Catal. B: Environ.* **95**, 160–168. (doi:10.1016/j.apcatb.2009.12.023)
25. Xi YZ, Ottinger NA, Liu ZG. 2014 New insights into sulfur poisoning on a vanadia SCR catalyst under simulated diesel engine operating conditions. *Appl. Catal. B: Environ.* **160–161**, 1–9. (doi:10.1016/j.apcatb.2014.04.037)
26. Song LY, Chao JD, Fang YJ, He H, Li J, Qiu WG, Zhang GZ. 2016 Promotion of ceria for decomposition of ammonia bisulfate over V_2O_5-MoO_3/TiO_2 catalyst for selective catalytic reduction. *Chem. Eng. J.* **303**, 275–281. (doi:10.1016/j.cej.2016.05.124)
27. Fang L, Hou L, Zhang Y, Wang Y, Yan G. 2017 Synthesis of highly hydrophobic rutile titania-silica nanocomposites by an improved hydrolysis co-precipitation method. *Ceram. Int.* **43**, 5592–5598. (doi:10.1016/j.ceramint.2017.01.091)
28. Pan FM, Zhang B, Cai WH. 2017 The effect of hydrophilicity/hydrophobicity of TiO_2-SiO_2 composite aerogels in the epoxidation reaction. *Catal. Commun.* **98**, 121–125. (doi:10.1016/j.catcom.2017.05.002)
29. García-Pérez UM, Martínez-de la Cruz A, Peral J. 2012 Transition metal tungstates synthesized by co-precipitation method: Basic photocatalytic properties. *Electrochim. Acta* **81**, 227–232. (doi:10.1016/j.electacta.2012.07.045)
30. Kompio PGWA, Brückner A, Hipler F, Auer G, Löffler E, Grünert W. 2012 A new view on the relations between tungsten and vanadium in V_2O_5-WO_3/TiO_2 catalysts for the selective reduction of NO with NH_3. *J. Catal.* **286**, 237–247. (doi:10.1016/j.jcat.2011.11.008)
31. Ettireddya PR, Ettireddya N, Mamedovb S, Boolchandc P, Smirniotis PG. 2007 Surface characterization studies of TiO_2 supported manganese oxide catalysts for low temperature SCR of NO with NH_3. *Appl. Catal. B: Environ.* **76**, 123–134. (doi:10.1016/j.apcatb.2007.05.010)
32. Fang D, Xie JL, Hu H, Yang H, He F, Fu ZB. 2015 Identification of MnO_x species and Mn valence states in MnO_x/TiO_2 catalysts for low temperature SCR. *Chem. Eng. J.* **271**, 23–30. (doi:10.1016/j.cej.2015.02.072)
33. Fang J, Bi XZ, Si DJ, Jiang ZQ, Huang WX. 2007 Spectroscopic studies of interfacial structures of CeO_2–TiO_2 mixed oxides. *Appl. Surf. Sci.* **253**, 8952–8961. (doi:10.1016/j.apsusc.2007.05.013)
34. Sahu DR, Hong LY, Wang SC, Huang JL. 2009 Synthesis, analysis and characterization of ordered mesoporous TiO_2/SBA-15 matrix: effect of calcination temperature. *Microporous Mesoporous Mater.* **117**, 640–649. (doi:10.1016/j.micromeso.2008.08.013)
35. Hussain M *et al.* 2017 VOCs photocatalytic abatement using nanostructured titania-silica catalysts. *J. Environ. Chem. Eng.* **5**, 3100–3107. (doi:10.1016/j.jece.2017.06.014)
36. Lu WZ, Lu HF, Zhang ZK. 2019 Data from: TiO_2–SiO_2 supported $MnWO_x$ catalysts by liquid-phase deposition for low-temperature NH_3-SCR. Dryad Digital Repository. (doi:10.5061/dryad.74pj317)